PAPER

Check for updates

Engineering red-emitting multi-functional nanocapsules for magnetic tumour targeting and imaging†

Julie Tzu-Wen Wang, [ID] *[a] Umberto Martino,[a] Rehan Khan, [ID] [b] Maasoomeh Bazzar,[b] Paul Southern,[c] Dönüş Tuncel [ID] *[b] and Khuloud T. Al-Jamal [ID] *[a]

In this work we describe the formulation and characterisation of red-emitting polymeric nanocapsules (NCs) incorporating superparamagnetic iron oxide nanoparticles (SPIONs) for magnetic tumour targeting. The self-fluorescent oligomers were synthesised and chemically conjugated to PLGA which was confirmed by NMR spectroscopy, FT-IR spectroscopy and mass spectrometry. Hydrophobic SPIONs were synthesised through thermal decomposition and their magnetic and heating properties were assessed by SQUID magnetometry and calorimetric measurements, respectively. Magnetic nanocapsules (m-NCs) were prepared by a single emulsification/solvent evaporation method. Their *in vitro* cytotoxicity was examined in CT26 colon cancer cells. The formulated fluorescent m-NCs showed good stability and biocompatibility both *in vitro* and *in vivo* in CT 26 colon cancer models. Following intravenous injection, accumulation of m-NCs in tumours was observed by optical imaging. A higher iron content in the tumours exposed to a magnetic field, compared to the contralateral tumours without magnetic exposure in the same animal, further confirmed the magnetic tumour targeting *in vivo*. The overall results show that the engineered red-emitting m-NCs have great potential as multifunctional nanocarriers for multi-model bioimaging and magnetic-targeted drug delivery.

Introduction

Magnetic nanoparticles have been widely explored for their potential application in cancer diagnosis or therapy.[1,2] For example, they can be used as contrast agents for magnetic resonance (MR) imaging to distinguish neoplastic lesions from normal tissues, due to their intrinsic magnetic properties. They can also be utilised for magnetic drug delivery such as tumour-targeting. Superparamagnetic iron oxide nanoparticles (SPIONs) are particularly ideal in this regard since they can be highly magnetised upon exposure to an external magnetic field and do not exhibit magnetic properties once the magnetic field is removed, avoiding agglomeration.[3] SPIONs are usually produced as hydrophobic ferrofluid solution and need

to be coated or encapsulated to be water-dispersible for intravenous injection. We have previously developed polymeric magnetic nanocapsules (m-NCs) capable of triple-modal imaging (*i.e.* MR, optical and nuclear imaging).[4] NCs are nanoparticulate carriers composed of an oil core surrounded by a PEGylated-PLGA polymeric shell with lipophilic and/or hydrophilic surfactants present at the interface. These polymeric NCs serve as a versatile platform with the ability to load high amounts of water insoluble drug molecules/SPIONs/fluorescent probes into the oil core.[4–6] The polymeric formulation provides protection against enzymatic degradation and confers a greater physicochemical stability as a whole. Based on the enhanced permeability and retention (EPR) effect, the m-NCs were able to passively accumulate in solid tumours with a leaky vasculature.[7,8] The presence of SPIONs further facilitated magnetic targeting in tumours in mice when an external magnetic field was applied.[4,7–9] As a result, by encapsulating an anticancer drug, docetaxel, the m-NCs indeed significantly delayed tumour growth and reduced the systemic side effects compared to the free drug.[9]

In previous studies, we were able to dynamically visualise magnetic targeting of m-NCs within tumours and the vasculature by optical imaging with the aid of infra-red fluorescent probes indocyanine green (ICG)[4] and 1,1-dioctadecyl-

[a]School of Cancer and Pharmaceutical Sciences, Faculty of Life Science & Medicine, King's College London, UK. E-mail: tzu-wen.wang@kcl.ac.uk, khuloud.al-jamal@kcl.ac.uk
[b]Department of Chemistry and UNAM–National Nanotechnology Research Centre, Bilkent University, Turkey. E-mail: dtuncel@fen.bilkent.edu.tr
[c]UCL Healthcare and Biomagnetics Laboratories, Royal Institution of Great Britain, London, UK
†Electronic supplementary information (ESI) available. See DOI: 10.1039/d0bm00314j

tetramethyl indotricarbocyanine iodide (DiR)[7] incorporated into the oil phase of m-NCs. Small organic fluorescent molecules can be used as imaging probes; however, they suffer from photo-bleaching and are therefore not suitable for long time imaging, especially *in vivo*. Recently, intrinsically fluorescent polymers, capable of forming nanoparticulate systems, have been proposed as a new type of fluorophore which can be used for *in vitro* cell labelling and *in vivo* live imaging and in image-guided drug delivery.[10–14] It was also shown that drug molecules can be loaded onto the polymeric nanoparticles with high loading capacity due to the hydrophobic effect and favourable π–π interactions between the drug molecules and the conjugated oligomer or polymer chains.[15,16]

Although conjugated polymer nanoparticles can provide high drug loading capacity, biodegradation of large polymeric residues after the delivery can pose some problems. To this end, conjugated oligomers are attractive because they have short chains and well-defined molecular weights. Moreover, they exhibit a higher fluorescence quantum yield than their polymeric counterparts.[17,18] However, one drawback is their lower drug loading capacity compared to polymer nanoparticles. Thus, in this work, we applied a different approach and directly conjugated the carboxyl terminated PLGA to an amine functionalised red-emitting fluorescent oligomer through amide bond formation. The formulation of m-NCs with the encapsulation of SPIONs was optimised and characterised. Their organ biodistribution profiles and ability for magnetic tumour targeting following intravenous injection were assessed *in vivo* in CT 26 colon cancer models by optical imaging and iron content quantification. The engineered self-fluorescent m-NCs were capable of *in vivo* optical imaging and magnetic tumour targeting.

Results and discussion

Synthesis and characterisation of Oligomer 1, Oligomer 2 and PLGA-Oligomer

In order to synthesise PLGA-conjugated oligomers, firstly **Oligomer 1** and **Oligomer 2** were synthesised as shown in the reaction (Scheme 1). Monomer 1 (**M1**) and monomer 2 (**M2**) were prepared as reported previously[18] and subsequently the bromide groups of **M2** were substituted by azides to obtain **M3**. Thereafter, the Pd-catalyzed Heck coupling reaction between **M3** and 4,7-dibromobenzo[*c*]-1,2,5-thiadiazole afforded **Oligomer 1**. In order to have suitable functional groups to link covalently with the carboxyl terminated PLGA, the azide groups of **Oligomer 1** were reduced to primary amine groups using PPh3 to obtain **Oligomer 2**. Finally, PLGA was conjugated to **Oligomer 2** through amide bond formation using the DCC coupling reaction.

Due to the high molecular weight of PLGA (Av. MW, 18 kDa) compared to that of **Oligomer 2** (MW, 745 Da), only one arm of **Oligomer 2** was functionalised. Unreacted **Oligomer 2** and PLGA were removed by precipitating

PLGA-Oligomer solution in THF in a large excess of water–methanol mixture.

Monomers and oligomers were characterised fully, and their characterization data are provided in the ESI (Fig. 1 and S1–S3†). The formation of **Oligomers 1 and 2** was confirmed by NMR spectroscopy (Fig. 1 and S2A†), FT-IR spectroscopy (Fig. S2C and S3A†) and mass spectrometry (Fig. S2B and S3A†). In the IR-spectrum of **Oligomer 1** (Fig. S2C†), the peak due to azide stretching at 2100 cm^{-1} disappears upon the reduction of the azide groups to amines to form **Oligomer 2** (Fig. S3A†). Fig. 1 compares the ^{1}H-NMR spectra of **Oligomer 1**, **Oligomer 2** and **PLGA-Oligomer**. The ^{1}H-NMR spectrum of **PLGA-Oligomer** shows the peaks of PLGA protons and some peaks of the aliphatic protons of **Oligomer 2**. The peaks belonging to the aromatic protons of **Oligomer 2** are not clearly seen because of the dominance of the PLGA peaks. Another reason for this could be a decrease in the mobility of the aromatic backbone of **Oligomer 2** caused by the attachment of a bulky PLGA arm.

SPION synthesis and characterisation

SPIONs were synthesised through a high-temperature organic phase decomposition of an iron precursor.[19,20] In contrast to the widely used co-precipitation method pioneered by Massart *et al.* with reactions taking place at room temperature,[21] the high-temperature decomposition method was reported to be able to provide a greater control on the final size of the nanoparticles with a narrower size distribution.[22] Carrying out nucleation at 200 °C and growth reactions under reflux at ∼300 °C separately is the key to yield monodisperse and highly crystalline magnetic nanoparticles. In the present study, different time periods for nucleation and growth (30 min to 2 h) were applied to optimise the synthesis of Fe$_3$O$_4$ magnetic nanoparticles (NP1–NP5, Table S1†). By SQUID (superconducting quantum interference device) magnetometry, it was observed that the obtained hysteresis loops normalised by saturation magnetisation were identical among all NPs, indicating that varying the time of nucleation and growth did not significantly affect the magnetic properties of the synthesised Fe$_3$O$_4$ NPs (Fig. S4A†). The heating ability of the magnetic nanoparticles can be assessed by the quantification of the intrinsic loss power (ILP) values and the normalised energy dissipation rates, facilitating direct comparison when the measurements were performed under different conditions.[23] Typical ILP values for iron oxide nanoparticles were reported in the range from 0.17 to 3.12 nHm^2 kg^{-1} (ref. 24) or below 5 nHm^2 kg^{-1}.[25] The obtained ILP values (Fig. S4B and Table S1†) were relatively low (0.02–0.04 nHm^2 kg^{-1}) as expected due to small particle size, estimated to be smaller than 10 nm.[26] Thermogravimetric analysis (TGA) was carried out to measure the oleic acid coating on NP1–NP5 which is indicated as weight loss % as shown in Table S1.† It has been reported that the amount of surfactant adsorption on the Fe$_3$O$_4$ nanoparticles decreased when the size of the nanoparticles increased.[20] Since NP1 exhibited the lowest weight loss and the highest ILP value among all,
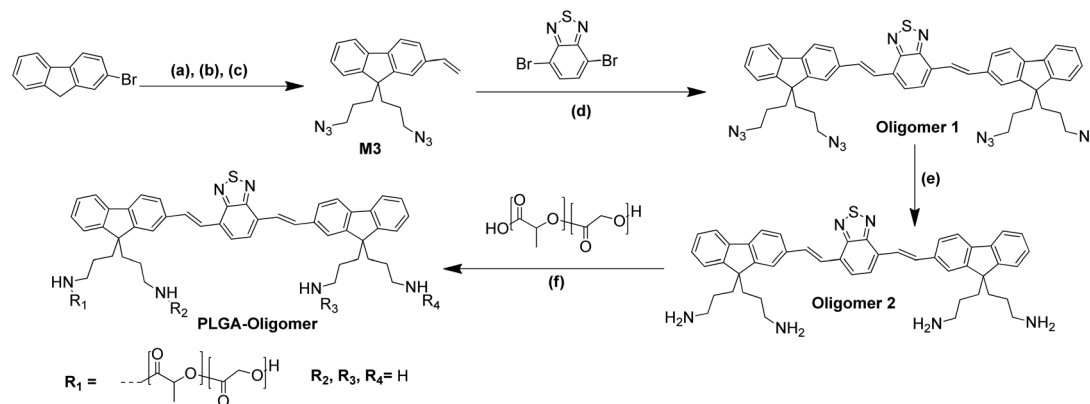
Scheme 1 Synthesis scheme for **PLGA-Oligomer**. (a) **M1**: 1,3-dibromopropane, aq. NaOH (50%, w/w), tetra-butyl ammonium bromide (TBAB), 80 °C, 64%, (b) **M2**: tributyl vinyltin, Pd(Cl$_2$)(PPh$_3$)$_2$, 2,6-di-*tert*-butyl phenol, toluene, 100 °C, 24 h, 90%, (c) **M3**: NaN$_3$, 60 °C, DMF, 24 h, 93%, (d) aq. K$_2$CO$_3$, Pd(OAc)$_2$, Pd(PPh$_3$)$_4$, DMF, 70 °C, 24 h, 45%, (e) PPh$_3$, THF, 25 °C, 24 h, 80%, and (f) 1-ethyl-3-(3-dimethylaminopropyl)carbodiimide (EDC), 4-dimethylaminopyridine (DMAP), 60 °C, DMF, 48 h, 78%.
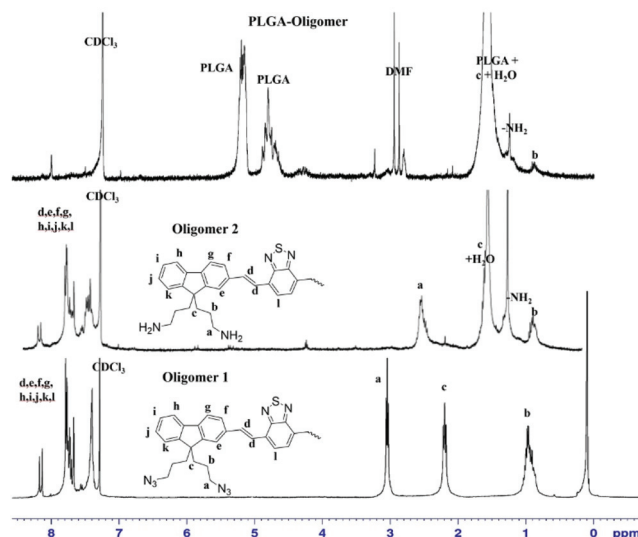

Fig. 1 ^{1}H-NMR (400 MHz, CDCl$_3$, 25 °C) spectra of **Oligomers 1, 2** and **PLGA-Oligomer**.

Fig. 2 Characterisation of the SPIONs synthesised by the seed mediated growth reaction (SMG) and SPION hybrid Fe/Co. (A) Magnetic property and (B) heating capacity assessments. Magnetization hysteresis curves were measured by SQUID magnetometry and normalised by the weight of the magnetic material. Calorimetric measurements were performed using a radio frequency amplifier.

further seed mediated growth (SMG) reaction (see Experimental), known to increase the diameter of the nanoparticles by ~2 nm per cycle,[19] was performed on NP 1 to increase the size of the SPIONs and presumably their heating ability. The same synthesis conditions (*i.e.* nucleation for 1 h and growth for 30 min) were used in the SMG reaction. For comparison, a parallel approach was carried out to produce Fe/Co hybrid nanoparticles in a single step method which are expected to possess enhanced heating properties due to increased magnetic anisotropy.[27]

NP 1 is named SPION 1 hereafter and SPIONs 2–3 were prepared by subjecting NP 1 to further 1–2 cycles of SMG respectively. The magnetic and heating properties of SPIONs 1–3 and the hybrid SPION Fe/Co were assessed (Fig. 2). No shift in hysteresis was present, indicating that their superparamagnetic behaviours were maintain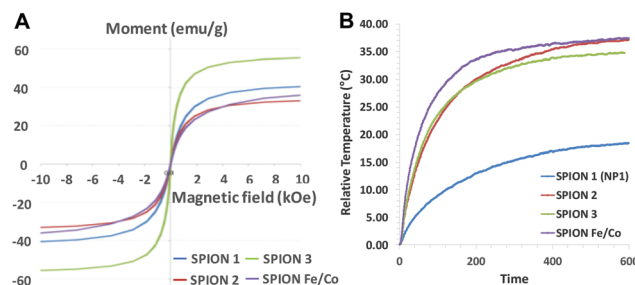ed, and their sizes are under the superparamagnetic/ferromagnetic threshold (Fig. 2A). SPIONs produced by SMG exhibited significantly higher ILP values (0.271 and 0.533 nHm^2 kg^{-1} for SPION 2 and SPION 3, respectively) than SPION 1 (0.043 nHm^2 kg^{-1}) and the hybrid SPION Fe/Co (0.178 nHm^2 kg^{-1}) (Table 1). Since its ILP value fell into the range reported in the literature, SPION 3 was chosen to formulate the magnetic polymeric nanocapsules in the subsequent studies.

Table 1 Heating properties of SPIONs

SPIONs	Intrinsic loss power[a] (ILP, nHm^2 kg^{-1})
SPION 1 (NP1)	0.04
SPION 2	0.27
SPION 3	0.53
SPION Fe/Co	0.18

[a] The calculation of ILP values were based on the iron content measured by ICP-MS and did not account for the oleic acid coating. The values were therefore lower than the actual values.

PLGA nanocapsule formulation and characterisation

Nanocapsules were formulated by an emulsification/solvent evaporation method. Initial formulation was optimised by mixing PLGA with an increasing amount of **PLGA-Oligomer** (10, 20 and 50% of total polymers). The results of the size and zeta potential measurements of the formulated nanocapsules are shown in Table S2.† It was found that increasing the percentage of **PLGA-Oligomer** led to increased particle size and surface charge (less negative) and the nanocapsules composed of 50% **PLGA-Oligomer** were the largest in size (>300 nm) among the three nanocapsules. Nevertheless, all formulations showed good stability in which no significant changes in the size and zeta potential were observed after storage at 4 °C for 1 week (data not shown). After purification by using PD-10 columns, tetrahydrofuran was added to the collected nanocapsules to break down the particles and dissolve the polymers. The optical properties of NCs, **Oligomer 2** and **PLGA-Oligomer** were assessed by UV-Vis spectroscopy and fluorimetry (Fig. S5†). It should be noted that NCs were dispersed in PBS, while **Oligomer 2** and **PLGA-Oligomer** were dissolved in THF. From the fluorescence spectra (Fig. S5B†), **Oligomer 2** and **PLGA-Oligomer** displayed the same emission maximum at 580 nm and there was a red shift for NCs with the emission maximum at 590 nm. By measuring the fluorescence intensity of **PLGA-Oligomer** extracted from the nanocapsules (calibration curves shown in Fig. S5C†), nearly 100% recovery was obtained in the polymer solutions, indicating that the entire amount of **PLGA-Oligomer** was incorporated into the nanocapsule formulations (data not shown). Nanocapsules composed of 20% **PLGA-Oligomer** of total polymers, with compromised properties in terms of size, stability and fluorescence intensity, were chosen for further PLGA-PEG magnetic nanocapsule formulation.

Magnetic PLGA-PEG nanocapsule formulation and characterisation

Magnetic polymeric nanocapsules consisting of PLGA-PEG (80%), **PLGA-Oligomer** (20%) and SPION 3 were formulated using the emulsification/solvent evaporation method. The formulated nanocapsules are named m-NCs hereafter. The counterpart formulation without SPIONs was also formulated, named NCs hereafter. The composition, size and zeta potential measurements of NCs and m-NCs are shown in Table 2. Inclusion of SPIONs slightly increased the size but did not affect the zeta potential of the nanocapsules. The size of NCs and m-NCs was in the range of 230–250 nm, larger than that
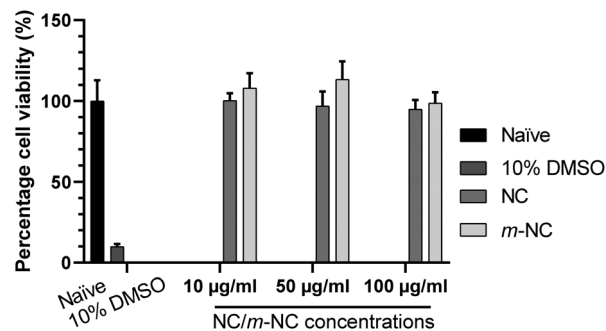

Fig. 3 *In vitro* cytotoxicity assessments. CT26 cells were incubated with NCs and m-NCs at the polymer concentrations of 10, 50 and 100 μg ml^{-1}. Cell viability was assessed by MTT assay after 72 h incubation.

of the m-NCs reported in our previous study (∼200 nm).[4] High encapsulation efficiency (EE%) of SPIONs was determined by ICP-MS in which nearly ∼90% SPION EE% was achieved.

In vitro cytotoxicity studies

The cytotoxic effect of NCs and m-NCs was assessed in CT26 cells using MTT assay prior to *in vivo* studies. As expected from our previous study,[9] no significant toxicity was observed in cells treated with either NCs or m-NCs up to the polymer concentration of 100 μg ml^{-1} for 72 h (Fig. 3).

In vivo optical imaging with magnetic targeting

For *in vivo* studies, NC and m-NC solutions were concentrated to 10× and buffered with 10× PBS for injection. Physicochemical characterisation showed that the size of NCs or m-NCs was within the range of 210–240 nm (Table S3†). Prior to *in vivo* imaging, the optical properties of NC and m-NC solutions were tested on a well plate at different concentrations up to 500 μg ml^{-1} using an IVIS Lumina III optical imaging system. This was performed considering that the previously reported oligomer has never been used for *in vivo* imaging.[18] A linear regression was performed for both NC and m-NC solutions with 500 nm/620 nm as the excitation/emission wavelength. Expectedly, due to the presence of SPIONs, fluorescence quenching was observed in m-NCs as signals were lower compared to those in NCs at the same polymer concentration which was more obvious at higher concentrations (Fig. S6†).

CT26 tumour-bearing Balb/c mice were intravenously injected with NCs or m-NCs. A permanent magnet (0.515 T)

Table 2 Physicochemical characterisation of different formulations of fluorescent NCs and m-NCs prepared by the emulsification/solvent evaporation method

Name	PLGA-PEG	**PLGA-Oligomer**	SPION 3	Diameter[a] (nm)	PDI[a]	Zeta potential[a] (mV)	EE[b] (%)
NC	80%	20%		236.3 ± 4.8	0.208	−13.9 ± 1.2	—
m-NCs	80%	20%	2.5 mg	251.1 ± 3.8	0.221	−13.2 ± 0.2	89.3

[a] Measurements were performed by dynamic light scattering in 10 mM NaCl (n = 3). [b] Iron content was determined by ICP-MS (n = 3).

was placed at one side of the tumours (TU$^+$) for 1 h. The contra-lateral tumour (TU$^-$) was used as an internal control where no magnetic field was applied. The animals behaved normally without any weight changes for up to 24 h after receiving a single intravenous injection of NCs or m-NCs. Increasing signals in tumours were observed over time up to 24 h although differences between TU$^+$ and TU$^-$ were not obvious by whole-body imaging (Fig. 4A). *Ex vivo* images of tissues excised at 24 h post injection confirmed the uptake of NCs and m-NCs in tumours (Fig. 4B and S7†). NCs and m-NCs had similar biodistribution patterns in general in which the particles accumulate in the liver as well as in other organs such as spleen, lungs, kidneys and intestine/colon. Quantitative analysis showed higher but insignificant signals detected in the tumours that had received 1 h magnetic exposure (TU$^+$) compared to non-treated tumours (TU$^-$) in both groups of mice injected with NCs or m-NCs (Fig. 4C).

Decreased fluorescence for the m-NC group compared to the NC group was observed, more significantly in TU$^+$ treatment (p = 0.01). This suggested the possibility of false negative results due to fluorescence quenching of the oligomer by SPIONs. It was deemed necessary to verify magnetic targeting by another method based on the quantification of SPION by ICP-MS.

Quantification of the iron content in tissues by ICP-MS

ICP-MS analysis of the iron content in tissues was further performed to assess the magnetic targeting in tumours considering that the fluorescence of the oligomer was significantly quenched by SPIONs. Samples from naïve mice were also processed to determine the intrinsic iron levels in these tissues. Fig. 5 presents the iron content per g of tissues. In the mice injected with m-NCs, the highest amount of iron was detected in the spleen and liver which already contain the highest amount of intrinsic iron (black bars). The intrinsic amount of iron in CT26 tumours was low (32.8 µg Fe per g of tumour) while a significant increase was observed in the tumours from the mice injected with m-NCs (zoom-in graph, Fig. 5). Moreover, the tumours that had been exposed to a magnetic field for 1 h (TU$^+$) showed a significantly higher iron content than the tumours without magnetic exposure (TU$^-$) (507.6 ± 6.7 *vs.* 362.0 ± 41.9 µg Fe per g, p = 0.04). The results indicate the magnetic targeting effects on increasing the tumour uptake of m-NCs. The fact that m-NCs reached the tumours and achieved magnetic targeting with increased tumour uptake also suggests that m-NCs were stable enough *in vivo* after intravenous injection.

The multifunctional features of SPIONs have shown great promise in a wide range of biomedical applications. Moreover, many SPION-based nanoconstructs have been
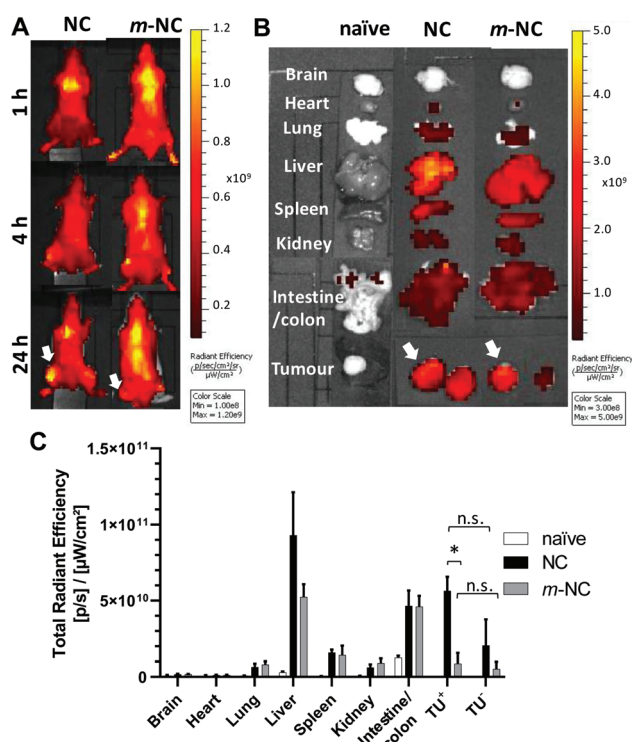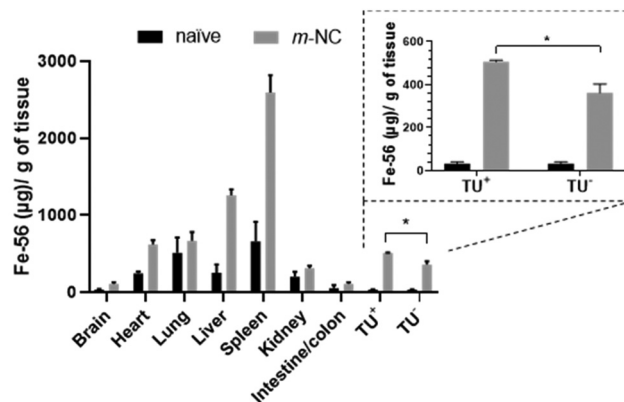

Fig. 4 *In vivo* whole-body optical imaging and *ex vivo* biodistribution of NCs and m-NCs in CT26 tumour-bearing Balb/c mice after intravenous administration. (A) Representative whole-body images from dorsal view of the mice at 1, 4 and 24 h post injection. (B) Representative *ex vivo* images of tissues excised at 24 h post injection. (C) Semi-quantitative analysis of the uptake of NCs and m-NCs in major tissues at 24 h post injection. Balb/c mice were transplanted subcutaneously with CT26 tumours at the lower flanks. When tumours reached ~7–8 mm in diameter, the mice were *i.v.* injected with NCs or m-NCs (250 mg polymer per kg and 50 mg SPION per kg). A magnetic field was applied by placing a permanent magnet (0.515 T) at the tumour site on the left side (TU$^+$) for 1 h (pointed by arrows). All images were obtained using an IVIS Lumina III optical imaging system (λ_{ex}: 500; λ_{em}: 620 nm). Data were analyzed by Living Image® 4.3.1 Service Pack 2 software. Data are presented as mean ± S.D. (n = 3). *p = 0.01 (one-way ANOVA).

Fig. 5 ICP-MS analysis of SPION uptake in CT26 tumour-bearing mice treated with m-NCs. CT26-bearing Balb/c mice were i.v. injected with m-NCs (250 mg polymer per kg and 50 mg SPION per kg) and a permanent magnet (0.515 T) was placed on one side of the tumour (TU$^+$) but not on the other side (TU$^-$) for 1 h. At 24 h post injection, major organs and tumours were excised and proceeded with ICP-MS analysis as described in Experimental. The data are expressed as iron content per g of tissues (dried weight) as mean ± S.D. (n = 3). *p = 0.04 (one-way ANOVA).

developed in which SPIONs were encapsulated or integrated with other materials to improve their hydrophilicity and biocompatibility.[28,29] The present study demonstrated an effective and robust approach to encapsulate high amounts of hydrophobic SPIONs in the hydrophobic compartment of the polymeric emulsion. The NCs and m-NCs developed in this study share many common features with the NC formulations published in our previous studies.[4,7,9] Apart from the inclusion of fluorescent **PLGA-Oligomer** and the replacement of SPIONs with the heating property, the use of other excipients (*e.g.* PLGA-PEG, oil, surfactants) and the formulation method/parameters were intended to remain unchanged to inherit the excellent fundamental physiochemical properties and the favourable *in vivo* behaviours. Indeed, the resulting NCs/ m-NCs exhibit characteristics typical of coil-cored PEGylated NCs including good colloidal stability, high SPION loading, and prolonged blood circulation thus passively enhancing tumour uptake. The resulting stable magnetic nanocapsules indeed exhibited improved water dispersity, prolonged blood circulation, and little or no toxicity *in vitro* and *in vivo* which are inherited from the PLGA-PEG polymers. By substitution of 20% PLGA-PEG polymers with the red-emitting macromolecule conjugate consisting of an oligomer backbone with PLGA polymer chains, the engineered self-luminescent NCs and m-NCs enabled direct visualisation of their kinetic tumour accumulation over time after administration by *in vivo* optical imaging. This is different from our previous studies using conventional approaches of either encapsulating or labelling with fluorescent probes for NCs/m-NCs, in which the labelling stability and dissociation of the dye from the nanocarriers should be taken into account while assessing biodistribution profiles by imaging.[4,7] Autofluorescence from tissues are expected which is mainly in green and red regions if excited with blue light. Considering the excitation for the fluorescent NCs and m-NCs at 500 nm (blue light), the obtained emission signals at 620 nm were rather satisfactory. In fact, the pilot *in silico* imaging in a well-plate has indirectly predicted the capability of the formulated m-NCs for *in vivo* detection. The highest dose tested in the well-plate (500 µg ml^{-1}) was equivalent to 1% injection dose (ID) for the *in vivo* studies (*i.e.* 1% ID contains 50 µg of polymer) whose signals of 1×10^{10} photos per sec were distinct from the background fluorescence and the likelihood of tissue autofluorescence signals usually below 10^9 photos per sec (Fig. S6†). The fluorescent **PLGA-Oligomer** and its nanocapsule formulation seemed to exhibit a relatively high signal-to-noise ratio, indicating the capability for optical imaging *in vivo* or in the clinic.

Hyperthermia is a promising tumour treatment and studies have developed magnetic nanoparticles for hyperthermia by means of photothermal ablation agents when irradiated with a NIR laser[30] or induce magnetic hyperthermia in the presence of an alternating magnetic field.[31] The SPIONs synthesised in the present study displayed desirable heating properties and evident magnetic tumour targeting, which open up a feasible future application of the developed m-NCs as a hyperthermia agent.

Conclusions

In conclusion, the resultant fluorescent m-NCs showed desirable magnetic and heating properties and exhibited good stability and biocompatibility both *in vitro* and *in vivo*. Following intravenous injection, accumulation of m-NCs in tumours was observed by optical imaging. A higher iron content in the tumours exposed to a magnetic field, compared to the contralateral tumours without magnetic exposure in the same animal, further confirmed their magnetic tumour targeting *in vivo*. The developed red-emitting functionalised m-NCs have great potential as an image-guided delivery system capable of magnetic-induced heating. Evaluation of the ability of the developed m-NCs for hyperthermia and encapsulation of chemotherapeutic drug will be the focus of future studies.

Experimental

Materials

All the chemicals used were of analytical grade, obtained from commercial suppliers and used as received without further purification. D/L-Lactide/glycolide copolymer 75/25 (PLGA$_{18 \text{ kDa}}$-COOH) was purchased from Purac Biomaterials (Netherlands). Soybean lecithin (Epikuron 140 V) was a kind gift from Cargill Pharmaceuticals (USA). D/L-Lactide/glycolide copolymer 75/25 (PLGA$_{18 \text{ kDa}}$-COOH) was purchased from Corbion Biomaterials (PURASORB® products, the Netherlands). PLGA-NH-PEG was synthesised as previously described.[5] Tween® 80 was obtained from Fisher Scientific Ltd (UK). Iron(III) acetylacetonate, cobalt(II) acetylacetonate, 1,2 tetradecanediol, oleylamine, oleic acid, sodium chloride, castor oil, toluene, and benzyl ether were purchased from Sigma-Aldrich (UK). Black 96 well-plates were purchased from Fisher Scientific Ltd (UK). Disposable polystyrene cuvettes (for size and PDI) or capillary cells (for zeta potential) were obtained from Malvern Instruments, UK. PD-10 desalting columns were obtained from GE Healthcare Life Sciences (UK). Gibco cell culture reagents including RPMI-1640 medium, fetal bovine serum (FBS), Glutamax™, non-essential amino acids, penicillin/streptomycin, trypsin/EDTA, and phosphate buffered saline (PBS) were purchased from Thermo Fisher Scientific Inc. 3-(4,5-Dimethylthiazol-2-yl)-2,5-diphenyltetrazolium bromide (MTT) was purchased from Sigma-Aldrich (UK).

Synthesis of 9,9-bis(3-azidopropyl)-2-vinyl-9*H*-fluorene (M3)

2-Bromo-9,9-bis(3-bromopropyl)-9*H*-fluorene and (**M1**) 9,9-bis (3-bromopropyl)-2-vinyl-9*H*-fluorene (**M2**) were synthesized as reported previously.[18] NaN$_3$ (400 mg, 6.15 mmol) was suspended in 10 mL of DMSO in a round bottom flask and 9,9-bis(3-bromopropyl)-2-vinyl-9*H*-fluorene (**M2**) (600 mg, 1.38 mmol) was added into the flask. The reaction mixture was stirred at 60 °C for 24 h. After completion of the reaction, the solvent was removed under reduced pressure. The residue was washed with water several times and the collected solid was dried under reduced pressure. Yield: 460 mg, 93%. ^{1}H NMR

(400 MHz, CDCl$_3$, 25 °C) δ ppm: 0.88–0.96 (m, 4H), 2.11–2.15 (t, 4H), 2.98–3.02 (t, 4H), 5.30–5.32 (d, 1H), 5.81–5.86 (d, 1H), 6.79–6.86 (m, 1H), 7.35–7.73 (m, 7H).

Synthesis of Oligomer 1

9,9-Bis(3-azidopropyl)-2-vinyl-9H-fluorene (516 mg, 1.44 mmol) and 4,7-dibromobenzo[c][1,2,5]thiadiazole (207 mg, 0.72 mmol) were placed in a two-necked round bottom flask and dried under vacuum for 30 min. 10 mL dry and degassed dimethylformamide (DMF) was added and stirred to complete dissolution. Aqueous solution of K$_2$CO$_3$ (486 mg, 3.51 mmol) was added into the flask. The mixture was subjected to a freeze–thaw-pump cycle 3 times to remove oxygen. Catalytic amounts of Pd(OAc)$_2$ (25.3 mg, 0.11 mmol) and Pd(PPh$_3$)$_4$ (26 mg, 0.02 mmol) were added under N$_2$ flow and the reaction mixture was heated to 70 °C for 24 h with constant stirring under N$_2$ flow. After completion of the reaction, the solvent was removed under reduced pressure. The crude product was dissolved in dichloromethane (DCM) and extracted with water several times. The organic phase was dried and further purified by column chromatography using diethyl ether as an eluent. Yield: 423 mg, 45%. ^{1}H NMR (400 MHz, CDCl$_3$, 25 °C) δ ppm: 0.87–1.00 (m, 8H), 2.08–2.13 (m, 8H), 2.97–3.05 (d, 8H), 7.00–7.87 (m, 20H). ^{13}C NMR (400 MHz, CDCl$_3$, 25 °C) δ ppm: 23, 30, 38, 52, 54, 119, 120, 120.53, 121, 122, 123, 124, 126, 127, 128, 129.12, 134.1, 138, 141, 142, 149, 160. ESI-MS (m/z): calcd for C$_{48}$H$_{44}$N$_{14}$S [M + H]$^+$: 849.36, found: 849.36.

Synthesis of Oligomer 2

Oligomer 1 (200 mg, 0.236 mmol) was dissolved in tetrahydrofuran (THF) (10 mL) and then the solution of PPh$_3$ (370 mg, 1.48 mmol) in THF (5 mL) was added. The resulting mixture was stirred for 24 h at room temperature. Water (10 mL) was then added and stirred for 24 h. THF was removed under reduced pressure and the precipitates were collected by filtration. The solid was washed with diethyl ether several times and then dried under reduced pressure. Yield: 140 mg, 80%. ^{1}H NMR (400 MHz, CDCl$_3$, 25 °C) δ ppm: 0.87–1.00 (m, 8H), 1.5–1.8 (m, 8H), 2.5 (m, 8H), 7.00–7.87 (m, 20H). ESI-MS (m/z): calcd for C$_{48}$H$_{52}$N$_6$S [M + H]$^+$: 745.40, found: 745.40.

Synthesis of PLGA-Oligomer

Oligomer 2 (70 mg, 0.094 mmol) was dissolved in dry DMF (6 mL) and 1-ethyl-3-(3-dimethylaminopropyl)carbodiimide (EDC) (73 mg, 0.47 mmol) and 4-dimethylaminopyridine (DMAP) (29 mg, 0.24 mmol) were added. The mixture was stirred for 5 min before the addition of PLGA (300 mg). The resulting mixture was further stirred at 60 °C under N$_2$ (g) for 48 h. After the completion of the reaction, the solvent was removed under reduced pressure and the residue was washed with water several times and then dried *in vacuo*. Yield: 290 mg, 78%.

NMR, LC-MS and UV-Vis characterisation and instrumentation

All ^{1}H and ^{13}C NMR spectra were recorded at room temperature using a Bruker Avance III 400 MHz NMR spectrometer. CDCl$_3$ purchased from Merck was used as the NMR solvent. Chemical shifts are reported in ppm. Mass analyses were performed with an Agilent 6210 LC/MS TOF mass spectrometer. Optical characterization was performed using a Cary 300 UV-Vis spectrophotometer and a Cary Eclipse fluorescence spectrophotometer.

SPION synthesis

The synthesis of SPIONs was performed by high-temperature degradation of iron(III) acetylacetonate as reported in the literature.[19,20] Fe(acac)$_3$ (2 mmol), 1,2-tetradecanediol (10 mmol), oleic acid (6 mmol), oleylamine (6 mmol), and benzyl ether (20 mL) were mixed and magnetically stirred under N$_2$ flow. For the synthesis of NP1, the mixture was heated to 200 °C for 1 h (nucleation reaction) and then, under a blanket of nitrogen, heated to reflux (298 °C, growth reaction) for another 30 min. The black-brown mixture was cooled to room temperature by removing the heat source. After the thermo-degradation reaction under ambient conditions, ethanol (40 mL) was added to the mixture and monodisperse Fe$_3$O$_4$ nanoparticles were obtained after centrifugation. The retrieved Fe$_3$O$_4$ nanoparticles were dissolved in hexane in the presence of oleic acid (∼0.05 mL) and oleylamine (∼0.05 mL). Centrifugation (6000 rpm, 10 min) was performed to remove any undispersed residue. The product, oleic acid-capped Fe$_3$O$_4$ nanoparticles, was then precipitated with ethanol, centrifuged (6000 rpm, 10 min) to remove the solvent, and re-dispersed in hexane, yielding NP1 (SPION 1). Different nucleation and growth times were used to synthesise NP2-NP5 and the details are described in Table S1.† SPION 1 dispersed in hexane was used as the seed to grow larger SPIONs in the Fe(acac)$_3$ precursor solution. Following the same workup procedures (*e.g.* nucleation/growth reaction and purification) described above, bigger oleic acid-capped Fe$_3$O$_4$ nanoparticles, *i.e.* SPION 2 (2 SMG steps) and SPION 3 (3 SMG steps), were produced.

As a control, reaction of Co(acac)$_2$ and Fe(acac)$_3$ (molar ratio of Co(acac)$_2$: Fe(acac)$_3$ was 1 : 4; 2 mM total metal salts) underwent 2 h nucleation and 1 h growth reaction, leading to hybrid CoFe$_2$O$_4$ nanoparticles which was also dispersed in hexane.

Superconducting quantum interference device (SQUID) magnetometry

The magnetic properties of the SPIONs were assessed by SQUID magnetometry. SPION samples (approx. 10 mg) were mounted using soft gelatin capsules and the magnetization curves were recorded at room temperature (300 K) using a Quantum Design (San Diego, USA) MPMS-VSM between ±7 Tesla.

Thermogravimetric analysis (TGA)

The amount of oleic acid coating on the SPIONs was characterised by thermogravimetric analysis (TGA) using a TGA Q500 (TA instrument). About 10 mg of SPIONs was loaded into a platinum pan and the measurement was pre-equilibrated at 80 °C and then heated from 100 °C to 800 °C with a temperature ramp of 10 °C min^{-1} under a compressed air atmosphere

with balance and sample purge flow rates of 10 and 90 ml min^{-1}, respectively.

Heating capability measurements

Calorimetric measurements were made using a radio frequency amplifier (Thamway T162-5723B) with a frequency range of 500–1000 kHz. The resonant circuit further consisted of a 20-turn water-cooled solenoid with an 8 cm diameter. The maximum AC magnetic field amplitude that could be generated was 13 kA m^{-1} at 930 kHz. A round-bottom-shaped plastic sample holder was used and surrounded by layers of insulation to protect the sample against ambient heating from the coil. Temperature measurements were conducted with fibreoptic temperature probes.[23]

NC and m-NC formulation

NCs and m-NCs were synthesised by the single emulsification/solvent evaporation method. Briefly, PLGA-PEG and **PLGA-Oligomer** mixture (12.5 mg), castor oil (75 mg), soybean lecithin (25 mg) and SPIONs (2.5 mg) were dissolved in 2.5 ml dichloromethane. Different ratios of PLGA-PEG and **PLGA-Oligomer** (weight percentage 90% : 10%, 80% : 20% and 50% : 50%, Table S2†) were used to formulate m-NCs. The organic phase was poured into an aqueous phase (5 ml, water) containing Tween® 80 (20 mg). The resulting dispersion was emulsified by ultra-sonication using a probe sonicator (Soniprep 150, UK) at 15 μm amplitude for 180 s in an ice bath, followed by organic phase evaporation in a chemical fume hood under stirring for 20 min. The formulated NCs and m-NCs were purified by size-exclusion chromatography (PD-10 column) using deionised water as the eluent to remove any unencapsulated SPION or materials that lack water solubility. The final volume of the NC and m-NC solutions was adjusted to 5 ml using a rotary evaporator at 40 °C.

Size and zeta measurements

The hydrodynamic size (Z-average), polydispersity index (PDI) and zeta potential of the formulated NCs and m-NCs were determined with a NanoZS (Malvern Instruments, UK) using disposable square polystyrene cuvettes (Malvern Instruments, UK) for the size and PDI, and disposable capillary cells (Malvern Instruments, UK) for the zeta potential at 25 °C. For size measurements, NC and m-NC solutions were diluted with deionised water or 10 mM NaCl. The Z-average diameter and polydispersity index were presented as the average value of three measurements, with 15 runs within each measurement. Electrophoretic mobility was used to calculate the zeta potential measurement. Three measurements were performed with 10–20 runs within each measurement.

SPION encapsulation efficiency measurements

The iron content in the hydrophobic SPION stock solutions and the SPION encapsulated in m-NCs were determined by inductively couple plasma mass spectrometry (ICP-MS) (PerkinElmer SCIEX ICP mass spectrometer, ELAN DRC 6100, USA). Fe standards (Leeman Labs Inc., MA) were prepared in 20% nitric acid to obtain a standard curve in the range of 10–10 000 parts per billion with respect to Fe. Different concentrations of SPION and m-NC solutions were digested in 67% nitric acid and incubated overnight at 50 °C. The resulting solution was diluted with deionised water before measurement. The iron content in non-purified NC solutions and purified NC solutions was measured to calculate the SPION encapsulation efficiency (EE%) in m-NCs.

In vitro cytotoxicity

CT26 murine colon carcinoma (CT26, ATCC®, CRL-2638™) cells were cultured in RPMI-1640 medium supplemented with 10% FBS, 50 U mL^{-1} penicillin, 50 μg mL^{-1} streptomycin, 1% GlutamaxTM and 1% non-essential amino acids. The cells were routinely grown in 75 cm^2 canted-neck tissue culture flasks and passaged twice a week using trypsin/EDTA at 80% confluency.

The CT26 cells were seeded in 96-well plates and incubated with NCs or m-NCs in complete media at polymer concentrations of 10, 50 and 100 μg mL^{-1} for 72 h. Cell viability was examined by MTT assay. Briefly, the culture medium was removed and replaced with 120 μL of MTT solution (at a concentration of 5 mg mL^{-1} in PBS with a further 1 : 6 dilution in media prior to use). The cells were incubated further for 3 h. The medium was removed, and the formed formazan was solubilised in 200 μL of DMSO. The absorbance was read at 570 nm using a FLUO star OPTIMA plate reader (BMG Labtech). Cell viability was calculated as a percentage of untreated control cells and expressed as mean ± S.D. ($n = 6$).

Animals and the tumour model

All animal experiments were performed in compliance with the UK Animals (Scientific Procedures) Act 1986 and UK Home Office Code of Practice for the Housing and Care of Animals Used in Scientific Procedures (Home Office 1989). *In vivo* experimentation adhered to the project licence approved by the King's College London animal welfare and ethical review body (AWERB) and UK Home Office. Female Balb/c mice aged 4–6 weeks were purchased from Envigo (UK) and used for all the *in vivo* experiments. CT26 cells were cultured as described above. Cells were harvested, resuspended in PBS and injected subcutaneously at the lower flanks of both sides of the mice.

Purified NC and m-NC solutions were further concentrated 10 times using a rotary evaporator and were adjusted to become isotonic by adding 10× PBS buffer solution. Disk neodymium magnets (8 mm in diameter, First4Magnets, UK) with a surface magnetic field flux density of 0.515 Tesla (0.5 T) were used for *in vivo* magnetic targeting studies.

In vivo optical imaging and organ biodistribution studies

Biodistribution studies were carried out when the tumours reached an appropriate size (~7–8 mm in diameter). CT26-bearing mice were subcutaneously injected with NC or m-NC solutions (250 mg polymer per kg and 50 mg SPION per kg). Immediately after injection, one magnet was placed non-invasively over the surface of the tumour implanted on the left

flank and retained using surgical tape. The contralateral tumour on the right side was used as an internal negative control where no magnetic field was applied. The magnet was removed at 1 h post-injection of the NCs or m-NCs. Optical imaging was performed using an IVIS® Lumina series III *In Vivo* Imaging Device (Caliper Life Sciences, PerkinElmer, USA). The images of the mice were captured at 1, 4 and 24 h post-injection. At 24 h post-injection, major organs (brain, heart, lungs, liver, spleen, kidneys, intestine/colon) and tumours were excised, weighed and imaged using the IVIS Lumina III optical imaging system (500/620 nm excitation/emission wavelengths) to assess the accumulation in tissues semi-quantitatively.

The iron accumulation in tissues was assessed quantitatively using ICP-MS. Tissues were dried, weighed and digested in 67% nitric acid and incubated overnight at 50 °C. The digested tissue solutions were diluted with deionised water and centrifuged at 4000g for 30 min. The supernatants were transferred into new tubes for ICP-MS analysis described previously.

Statistical analysis

Statistical significance between groups was determined using one-way ANOVA. Differences were considered statistically significant when p-values were less than 0.05.

Conflicts of interest

The authors declare no competing financial interest.

Acknowledgements

References

1 M. Arruebo, R. Fernández-Pacheco, M. R. Ibarra and J. Santamaría, Magnetic nanoparticles for drug delivery, *Nano Today*, 2007, **2**(3), 22–32.

2 M. Wu and S. Huang, Magnetic nanoparticles in cancer diagnosis, drug delivery and treatment, *Mol. Clin. Oncol.*, 2017, **7**(5), 738–746.

3 Z. Bakhtiary, A. A. Saei, M. J. Hajipour, M. Raoufi, O. Vermesh and M. Mahmoudi, Targeted superparamagnetic iron oxide nanoparticles for early detection of cancer: Possibilities and challenges, *Nanomedicine*, 2016, **12**(2), 287–307.

4 J. Bai, J. T.-W. Wang, N. Rubio, A. Protti, H. Heidari, R. Elgogary, P. Southern, W. T. Al-Jamal, J. Sosabowski and A. M. Shah, Triple-modal imaging of magnetically-targeted nanocapsules in solid tumours in vivo, *Theranostics*, 2016, **6**(3), 15.

5 R. I. El-Gogary, N. Rubio, J. T.-W. Wang, W. T. Al-Jamal, M. Bourgognon, H. Kafa, M. Naeem, R. Klippstein, V. Abbate and F. Leroux, Polyethylene glycol conjugated polymeric nanocapsules for targeted delivery of quercetin to folate-expressing cancer cells in vitro and in vivo, *ACS Nano*, 2014, **8**(2), 1384–1401.

6 R. Klippstein, J. T.-W. Wang, R. I. El-Gogary, J. Bai, F. Mustafa, N. Rubio, S. Bansal, W. T. Al-Jamal and K. T. Al-Jamal, Passively Targeted Curcumin-Loaded PEGylated PLGA Nanocapsules for Colon Cancer Therapy In Vivo, *Small*, 2015, **11**(36), 4704–4722.

7 J. Bai, J. T.-W. Wang, K.-C. Mei, W. T. Al-Jamal and K. T. Al-Jamal, Real-time monitoring of magnetic drug targeting using fibered confocal fluorescence microscopy, *J. Controlled Release*, 2016, **244**, 240–246.

8 K.-C. Mei, J. Bai, S. Lorrio, J. T.-W. Wang and K. T. Al-Jamal, Investigating the effect of tumor vascularization on magnetic targeting in vivo using retrospective design of experiment, *Biomaterials*, 2016, **106**, 276–285.

9 K. T. Al-Jamal, J. Bai, J. T. Wang, A. Protti, P. Southern, L. Bogart, H. Heidari, X. Li, A. Cakebread, D. Asker, W. T. Al-Jamal, A. Shah, S. Bals, J. Sosabowski and Q. A. Pankhurst, Magnetic drug targeting: Preclinical in vivo studies, mathematical modeling, and extrapolation to humans, *Nano Lett.*, 2016, **16**(9), 5652–5660.

10 G. Feng, Y. Fang, J. Liu, J. Geng, D. Ding and B. Liu, Multifunctional Conjugated Polymer Nanoparticles for Image-Guided Photodynamic and Photothermal Therapy, *Small*, 2017, **13**(3), 1602807.

11 D.-D. Li, J.-X. Wang, Y. Ma, H.-S. Qian, D. Wang, L. Wang, G. Zhang, L. Qiu, Y.-C. Wang and X.-Z. Yang, A Donor–Acceptor Conjugated Polymer with Alternating Isoindigo Derivative and Bithiophene Units for Near-Infrared Modulated Cancer Thermo-Chemotherapy, *ACS Appl. Mater. Interfaces*, 2016, **8**(30), 19312–19320.

12 D. Tuncel, π-Conjugated nanostructured materials: preparation, properties and photonic applications, *Nanoscale Adv.*, 2019, **1**(1), 19–33.

13 X. Xu, R. Liu and L. Li, Nanoparticles made of π-conjugated compounds targeted for chemical and biological applications, *Chem. Commun.*, 2015, **51**(94), 16733–16749.

14 J. Yu, Y. Rong, C.-T. Kuo, X.-H. Zhou and D. T. Chiu, Recent Advances in the Development of Highly Luminescent Semiconducting Polymer Dots and Nanoparticles for Biological Imaging and Medicine, *Anal. Chem.*, 2017, **89**(1), 42–56.

15 Ö. Gezici, İ. Durmaz, E. Bilget Güven, Ö. Ünal, A. Özgün, R. Cetin-Atalay and D. Tuncel, Dual functionality of conjugated polymer nanoparticles as an anticancer drug carrier and a fluorescent probe for cell imaging, *RSC Adv.*, 2014, **4**(3), 1302–1309.

16 J. Pennakalathil, A. Özgün, I. Durmaz, R. Cetin-Atalay and D. Tuncel, pH-responsive near-infrared emitting conjugated polymer nanoparticles for cellular imaging and con-

trolled-drug delivery, *J. Polym. Sci., Part A: Polym. Chem.*, 2015, **53**(1), 114–122.

17 I. Fischer, A. Kaeser, M. A. M. Peters-Gumbs and A. P. H. J. Schenning, Fluorescent π-Conjugated Polymer Dots versus Self-Assembled Small-Molecule Nanoparticles: What's the Difference?, *Chem. – Eur. J.*, 2013, **19**(33), 10928–10934.

18 J. Pennakalathil, E. Jahja, E. S. Özdemir, Ö. Konu and D. Tuncel, Red Emitting, Cucurbituril-Capped, pH-Responsive Conjugated Oligomer-Based Nanoparticles for Drug Delivery and Cellular Imaging, *Biomacromolecules*, 2014, **15**(9), 3366–3374.

19 S. Sun, H. Zeng, D. B. Robinson, S. Raoux, P. M. Rice, S. X. Wang and G. Li, Monodisperse MFe2O4 (M = Fe, Co, Mn) Nanoparticles, *J. Am. Chem. Soc.*, 2004, **126**(1), 273–279.

20 L. Zhang, R. He and H.-C. Gu, Oleic acid coating on the monodisperse magnetite nanoparticles, *Appl. Surf. Sci.*, 2006, **253**(5), 2611–2617.

21 R. Massart, Preparation of aqueous magnetic liquids in alkaline and acidic media, *IEEE Trans. Magn.*, 1981, **17**(2), 1247–1248.

22 S. Sun and H. Zeng, Size-Controlled Synthesis of Magnetite Nanoparticles, *J. Am. Chem. Soc.*, 2002, **124**(28), 8204–8205.

23 M. Kallumadil, M. Tada, T. Nakagawa, M. Abe, P. Southern and Q. A. Pankhurst, Suitability of commercial colloids for magnetic hyperthermia, *J. Magn. Magn. Mater.*, 2009, **321**(10), 1509–1513.

24 R. R. Wildeboer, P. Southern and Q. A. Pankhurst, On the reliable measurement of specific absorption rates and intrinsic loss parameters in magnetic hyperthermia materials, *J. Phys. D Appl. Phys.*, 2014, **47**(49), 495003.

25 F. Mérida, A. Chiu-Lam, A. C. Bohórquez, L. Maldonado-Camargo, M.-E. Pérez, L. Pericchi, M. Torres-Lugo and C. Rinaldi, Optimization of synthesis and peptization steps to obtain iron oxide nanoparticles with high energy dissipation rates, *J. Magn. Magn. Mater.*, 2015, **394**, 361–371.

26 J.-H. Lee, J.-T. Jang, J.-S. Choi, S. H. Moon, S.-H. Noh, J.-W. Kim, J.-G. Kim, I.-S. Kim, K. I. Park and J. Cheon, Exchange-coupled magnetic nanoparticles for efficient heat induction, *Nat. Nanotechnol.*, 2011, **6**, 418.

27 N. Lee, D. Yoo, D. Ling, M. H. Cho, T. Hyeon and J. Cheon, Iron Oxide Based Nanoparticles for Multimodal Imaging and Magnetoresponsive Therapy, *Chem. Rev.*, 2015, **115**(19), 10637–10689.

28 W. Wu, C. Z. Jiang and V. A. L. Roy, Designed synthesis and surface engineering strategies of magnetic iron oxide nanoparticles for biomedical applications, *Nanoscale*, 2016, **8**(47), 19421–19474.

29 L. Zhang, W.-F. Dong and H.-B. Sun, Multifunctional superparamagnetic iron oxide nanoparticles: design, synthesis and biomedical photonic applications, *Nanoscale*, 2013, **5**(17), 7664–7684.

30 B. Sivakumar, R. G. Aswathy, R. Romero-Aburto, T. Mitcham, K. A. Mitchel, Y. Nagaoka, R. R. Bouchard, P. M. Ajayan, T. Maekawa and D. N. Sakthikumar, Highly versatile SPION encapsulated PLGA nanoparticles as photothermal ablators of cancer cells and as multimodal imaging agents, *Biomater. Sci.*, 2017, **5**(3), 432–443.

31 G. Béalle, R. Di Corato, J. Kolosnjaj-Tabi, V. Dupuis, O. Clément, F. Gazeau, C. Wilhelm and C. Ménager, Ultra Magnetic Liposomes for MR Imaging, Targeting, and Hyperthermia, *Langmuir*, 2012, **28**(32), 11834–11842.